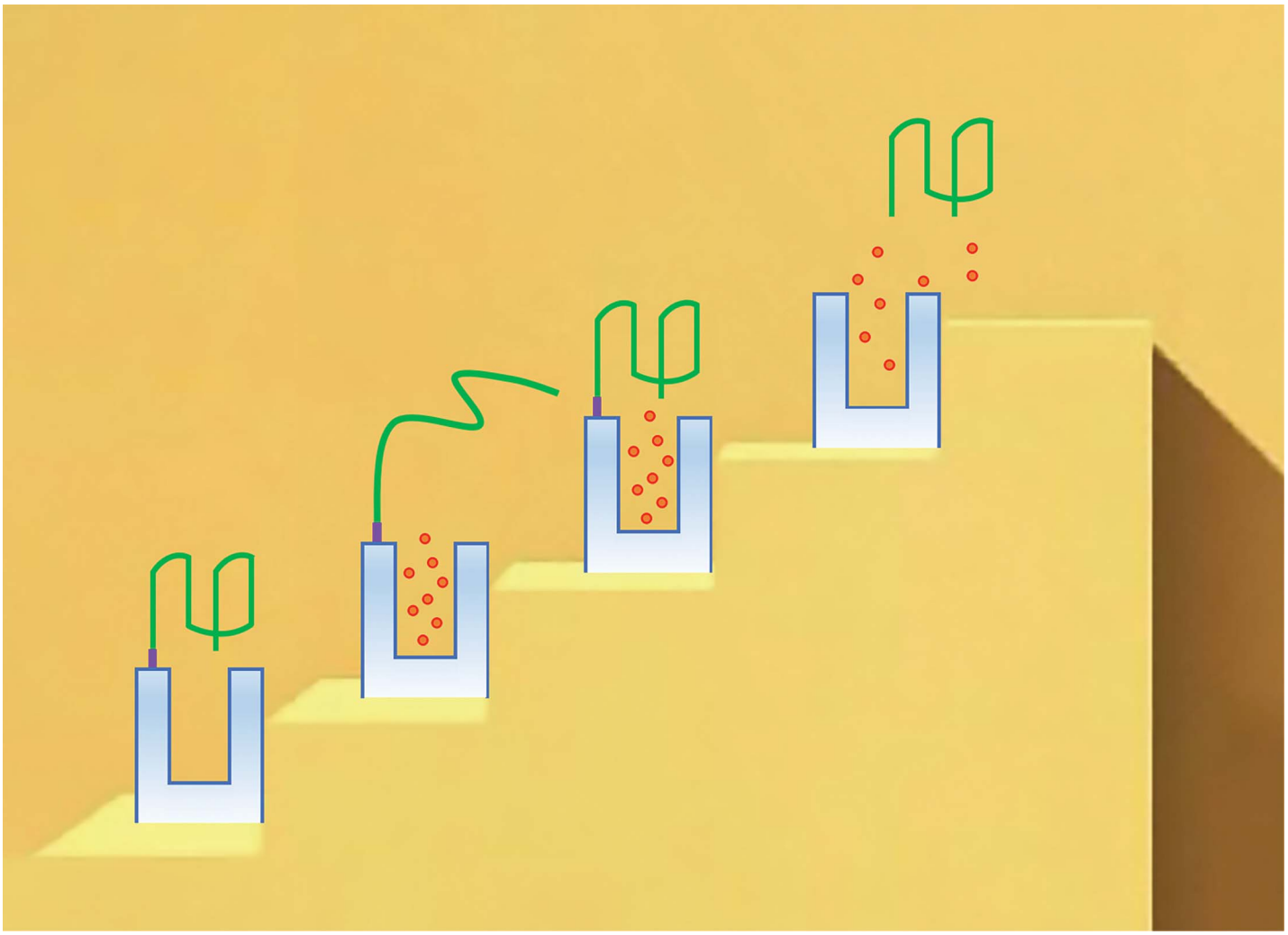

Showcasing research from Professor Yong Ma's laboratory, Department of Chemistry, School of Forensic Medicine, China Medical University, Shenyang, China.

Construction of a redox-responsive drug delivery system utilizing the volume of AS1411 spatial configuration gating mesoporous silica pores

A GSH-responsive drug delivery system was developed based on mesoporous silica with AS1411 aptamer capping the pore openings as nano-gatekeeper. We aimed to tell that the spatial volume of the G-quadruplex configuration of the AS1411 aptamer can be utilized to cap the pore of the drug-carrier, and discussed the stimulus-responsive controlled release behavior of this drug delivery system.

As featured in:

See Yong Ma *et al.*, *Nanoscale Adv.*, 2022, **4**, 4059.

ROYAL SOCIETY OF CHEMISTRY

rsc.li/nanoscale-advances

Registered charity number: 207890

Nanoscale Advances

ROYAL SOCIETY OF CHEMISTRY

PAPER

View Article Online
View Journal | View Issue

Cite this: *Nanoscale Adv.*, 2022, **4**, 4059

Construction of a redox-responsive drug delivery system utilizing the volume of AS1411 spatial configuration gating mesoporous silica pores†

Lu Zhou, [a] Yajie Zhang [b] and Yong Ma *[a]

In recent years, diverse redox-responsive drug delivery systems have emerged to prevent premature drug release and reduce drug toxicity in the human body in cancer treatment. In this paper, we put forward a view of directly utilizing the spatial structure size of the AS1411 aptamer as the nano-gatekeeper on the pore openings of MCM-41 type mesoporous silica and thus constructed a redox-responsive drug delivery system named MCM-41-SS-AS1411. The particles obtained at each step were characterized by TEM, FTIR, SXRD, TGA and zeta potential measurement. The characterization data confirmed that the particles were successfully prepared. The binding amount of the aptamer was *ca.* 3.1×10^3 for each carrier particle averagely. The anticancer drug Dox was regarded as a drug model to investigate the redox-controlled drug release behavior by fluorescence measurements. The investigation results demonstrate that the spatial volume of aptamer AS1411 can block the mesopore, and this drug-carrier can realize controlled drug release by GSH. We hope this idea can play a prompt role in relevant research. Meanwhile, the preparation steps of this DDS are simplified.

Received 11th July 2022
Accepted 18th August 2022

DOI: 10.1039/d2na00446a

rsc.li/nanoscale-advances

1. Introduction

Premature drug release has been a challenging problem in drug delivery systems (DDSs) used to overcome cancer. If this problem can be prevented, the side effects would be reduced, and drug efficacy would be improved. Hence the development of stimulus-responsive DDSs has received extensive attention in recent years. Some materials can encapsulate the drug molecules in carriers before the DDS reaches the target sites, and drugs will not be released in advance during transportation. Moreover, these materials can be affected by changes in pH,[1,2] redox,[3,4] enzymes,[5] temperature or light. Through such stimuli, drug molecules can be released. Redox is widely used as an endogenous stimulus. In redox stimulation, glutathione (GSH) which can break disulfide bonds (–S–S–) is an important reductant in biochemical reactions. The concentration of GSH was about 10 μM in extracellular fluid, while it was up to 1–10 mM in intracellular fluid.[6] And the concentration of GSH in the cytoplasm of most tumor cells is at least 3 times higher than that of normal cells.[7] The disulfide bonds can exist stably in extracellular fluid and be easily broken in intracellular fluid due to the significant difference in the concentration of GSH in intracellular and extracellular fluids. This feature can be used for stimulus-responsive DDSs.

Mesoporous silica nanoparticles (MSNs) are regarded as an ideal carrier for stimulus-responsive DDSs,[8] and MCM-41 is a commonly used type.[9] The pores of MCM-41 present a one-dimensional hexagonal highly ordered arrangement with various pore diameters from 1.5 to 10 nm.[9–11]

Researchers have proposed targeted controlled-release DDSs so as to deliver effective doses of drugs to target tumor cells or tissues,[12] reduce drug accumulations in healthy organs or tissues, and improve the biodistribution of drugs in the whole body. An aptamer is a kind of oligomeric single-stranded DNA (ssDNA) or RNA molecule with specific recognition function, which was selected through systematic evolution of ligands by exponential enrichment (SELEX) technology.[13–15] It can fold into a unique three-dimensional conformation through intramolecular interactions[14] and specifically bind to target molecules such as target polypeptides, protein receptors and intracellular biological macromolecules by its excellent affinity.[16] It also provides attractive characteristics such as small size, easy synthesis and modification, and low toxicity and immunogenicity, as well as high thermal stability. Therefore, it has become an ideal molecular probe for diagnosis and therapeutic applications.[17,18] The AS1411 aptamer is a kind of ssDNA with 26 bases (sequence: 5′-GGTGGTGGTGGT-TGTGGTGGTGGTGG-3′), which can selectively bind to nucleolin. Nucleolin is overexpressed on the surface of many cancer cells but not on normal ones. In recent years, there have been a few research studies on combining mesoporous silica and an

[a]*Department of Chemistry, School of Forensic Medicine, China Medical University, Shenyang 110122, China. E-mail: yma10@cmu.edu.cn*

[b]*Department of Gastroenterology, Shengjing Hospital of China Medical University, Shenyang 110004, China*

† Electronic supplementary information (ESI) available: More details of experimental procedures. See https://doi.org/10.1039/d2na00446a

aptamer. For example, Sa *et al.*[19] impregnated pores of SBA-15 with an aptamer (functionalized for the tumor marker MUC-1) and demonstrated the ability of the complex to bind and internalize into the cells. Nejabat *et al.*[20] coated the surface of doxorubicin-encapsulated HMSNs with acetylated carboxymethyl cellulose (Ac-CMC) and then covalently conjugated to the AS1411 aptamer for guided drug delivery to nucleolin. Li *et al.*[21] reported anti-miR-155-loaded MSNs modified with polymerized dopamine (PDA) and the AS1411 aptamer (MSNs-anti-miR-155@PDA-Apt) for the targeted treatment of CRC. Nevertheless, we intended to construct a DDS that could fill drug molecules in the silica pores and has multiple functions, such as stimuli-responsiveness, pore-capping and targeting cancer cells or tissues, but only a single coating is enough. Therefore, we put forward an idea of directly utilizing the spatial structure size of the AS1411 aptamer to cap the pore-opening of Dox-loaded mesoporous silica to simplify the preparation of the multifunctional DDS.

In the present work, MCM-41 type MSN was used as the drug carrier, and its surface was modified with –SH. The AS1411 aptamer modified with –SH at one end of its chain was bound to the Dox-loaded MSN through one disulfide bond. AS1411 forms a structure of G-quadruplex due to its rich G content, and the diameter of its spatial structure is 2–3 nm (ref. 22) which was suitable for capping the pore of the MSN (pore size 3–5 nm) used in this study. The aptamers will be separated, and the pores can open and release Dox when –S–S– is broken by glutathione. For one thing, the spatial volume of AS1411 can cap the pores so as to prevent premature drug release. For another, the prepared DDS can respond to GSH so that cargo molecules can be released in a tumor cell microenvironment. Moreover, aptamers are well known for their targeting characteristics and has attracted extensive attention, and the targeting effect of AS1411 has been confirmed by many research studies.[23–27] So it can be inferred that the concept of directly using AS1411 to cap the pores can provide many advantages. This DDS is expected to possess comprehensive features and functions simultaneously. But in this paper, we mainly focus on discussing the encapsulating effect of utilizing the spatial volume of AS1411 as well as the stimulus-responsive controlled release behavior of the DDS.

2. Results and discussion

2.1 TEM

The morphology of mesopores of MCM-41 and MCM-41-SS-AS1411 were determined by transmission electron microscopy (TEM) (Fig. 1). As can be seen from the figure, the pore channel is well ordered, and its average diameter is 3–5 nm. The change of the pore structure is hardly observed before and after AS1411 was grafted. Fig. S1† shows the particle size and morphology of MCM-41 and MCM-41-SS-AS1411.

2.2 FTIR

The FTIR spectra of MSNs are shown in Fig. 2. The spectrum of original MCM-41 is included for comparison. The band at around 1083 cm^{-1} is due to Si–O–Si stretching vibration, and the band at 799 cm^{-1} is due to Si–C. Compared with MCM-41, the weak new absorption peak at 2566 cm^{-1} is –SH[28] (red curve). And the new peak at 2933 cm^{-1} is caused by the asymmetric stretching vibration of $–CH_2–$ contained in the modified group which confirmed the formation of MCM-41-SH. Meanwhile, the weak band at around 966 cm^{-1} associated with Si–OH groups is present in the pure MCM-41 but disappears after modification with MPTMS. It also strongly reveals that –SH has been anchored on the surface of MCM-41 through the interaction with the surface silanol groups. These illustrate that the –SH groups have been successfully grafted on the surface of MCM-41 *via* covalent bonds. After DTDP reacted with MCM-41-SH, the spectrum of their product MCM-41-SS-Py is also shown in Fig. 2 as the blue curve. The characteristic absorption bands at around 1583, 1564, 1451 and 1421 cm^{-1} are attributed to the stretching vibrations of C=C and C=N bonds in the pyridine structures, respectively. New characteristic absorption peaks at 765 and 715 cm^{-1} are due to the out-of-plane vibration of C–H on the pyridine ring, which also proves the successful synthesis of these particles.

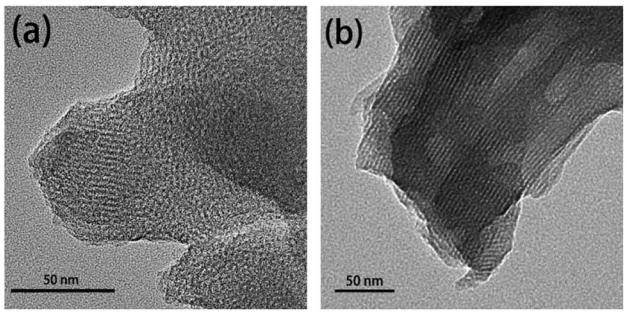

Fig. 1 TEM images of mesopores of (a) MCM-41; (b) MCM-41-SS-AS1411.

2.3 SXRD

As presented in Fig. 3, the small-angle X-ray diffraction (SXRD) patterns of MCM-41 exhibit the (100), (110) and (200) diffraction

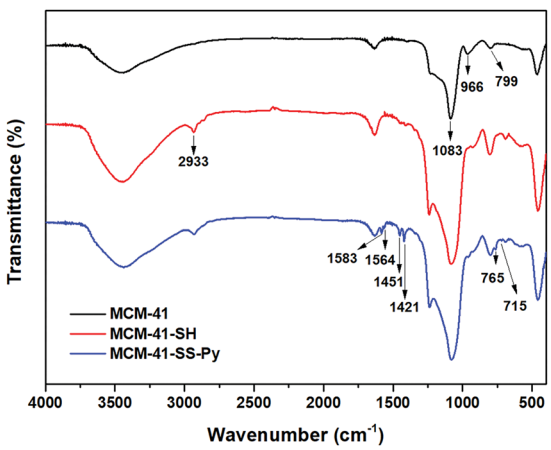

Fig. 2 FTIR spectra of MCM-41, MCM-41-SH and MCM-41-SS-Py.

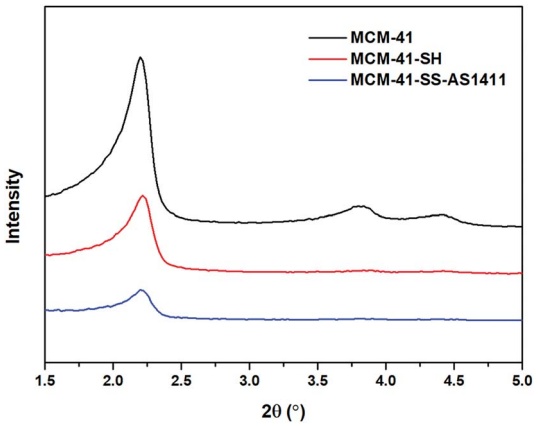

Fig. 3 SXRD patterns of MCM-41, MCM-41-SH and MCM-41-SS-AS1411.

peaks at $2\theta = 2.2$, 3.8 and 4.4°, respectively, which are typical features of a hexagonal unit cell, indicating that the raw material MCM-41 has a highly ordered hexagonal structure. After modification with –SH, the intensity of the (110) and (200) diffraction peaks decreases or even disappears compared with the original MCM-41, which decreases inevitably due to the order of channel structure after functionalization. With the further modification of SH-AS1411 aptamers, the intensity of the diffraction peak gets further decreased for the same reason. In addition, as can be seen from Fig. 3, the peak position of the (100) plane shifts slightly to the right with every modification, so the pore size of the carrier gets reduced slightly, indicating the successful modifications. The SXRD patterns prove that –SH and aptamers had been successfully modified on MCM-41. Meanwhile, the persistence of the (100) diffraction peak indicated that after functionalization of –SH and SH-AS1411, the particles still had a hexagonal structure.

2.4 TGA

Fig. 4 shows the TGA curves of MCM-41, MCM-41-SH and MCM-41-SS-AS1411 recorded in a N_2 flow at a heating rate of 10 °C min^{-1}. The weight loss of MCM-41 was very low. For MCM-41-SH, the weight loss is due to the loss of grafted organic groups. MCM-41-SS-AS1411 has a further weight loss which is caused by both –S–S– and AS1411 loss. These changes indicated that the aptamer had been grafted on MCM-41, and there was about 4.4 wt% AS1411 aptamer bonded to the MCM-41 surface *via* one disulfide bond.

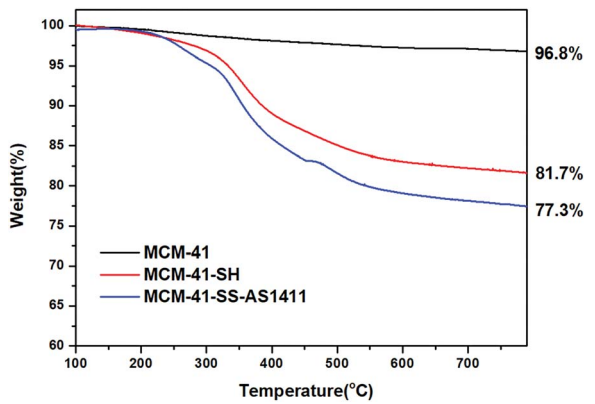

Fig. 4 TGA curves of MCM-41, MCM-41-SH and MCM-41-SS-AS1411.

Table 1 Zeta potentials of MCM-41, MCM-41-SH and MCM-41-SS-AS1411

Sample	Zeta potential (mV)
MCM-41	−42.20 ± 0.49
MCM-41-SH	−45.37 ± 3.01
MCM-41-SS-AS1411	−53.10 ± 0.21

Table 2 Aptamer binding amounts of each carrier particle

Carrier particle amount	Corresponding aptamer binding amount
1	~3.1×10^3

2.5 Measurement of the zeta potential

Dynamic light scattering (DLS) was used to measure the zeta potential of unloaded empty MSNs. The zeta potentials of MCM-41, MCM-41-SH and MCM-41-SS-AS1411 are as shown in Table 1, which are (−42.20 ± 0.49) mV, (−45.37 ± 3.01) mV and (−53.10 ± 0.21) mV, respectively. The thiol group has a negative charge, so the zeta potentials of MCM-41-SH got lower after the negatively charged MCM-41 was modified with –SH. Similarly, the further reduced zeta potential of MCM-41-SS-AS1411 was attributed to the negatively charged DNA aptamer. The zeta potential results also show that the AS1411 aptamer conjugated with MSNs.

2.6 Determination of the aptamer binding amount

According to the fluorescence intensity of the supernatant after the reaction, it was calculated that each milligram of MCM-41-SS-Py could bind about 0.55 nmol of SH-AS1411-Cy5. Then calculated by using formulas (1) and (2), the number of AS1411 aptamers binding to each carrier particle is *ca.* 3.1×10^3 averagely (Table 2).

2.7 Loading amount of Dox

Table 3 shows the loading mass of Dox per milligram of MSNs calculated by using formula (3) according to the result of

Table 3 Loading amount of Dox

Carrier	Loading amount of Dox (μg mg^{-1})
MCM-41	62.5 ± 17.1
MCM-41-SS-AS1411	93.5 ± 12.8

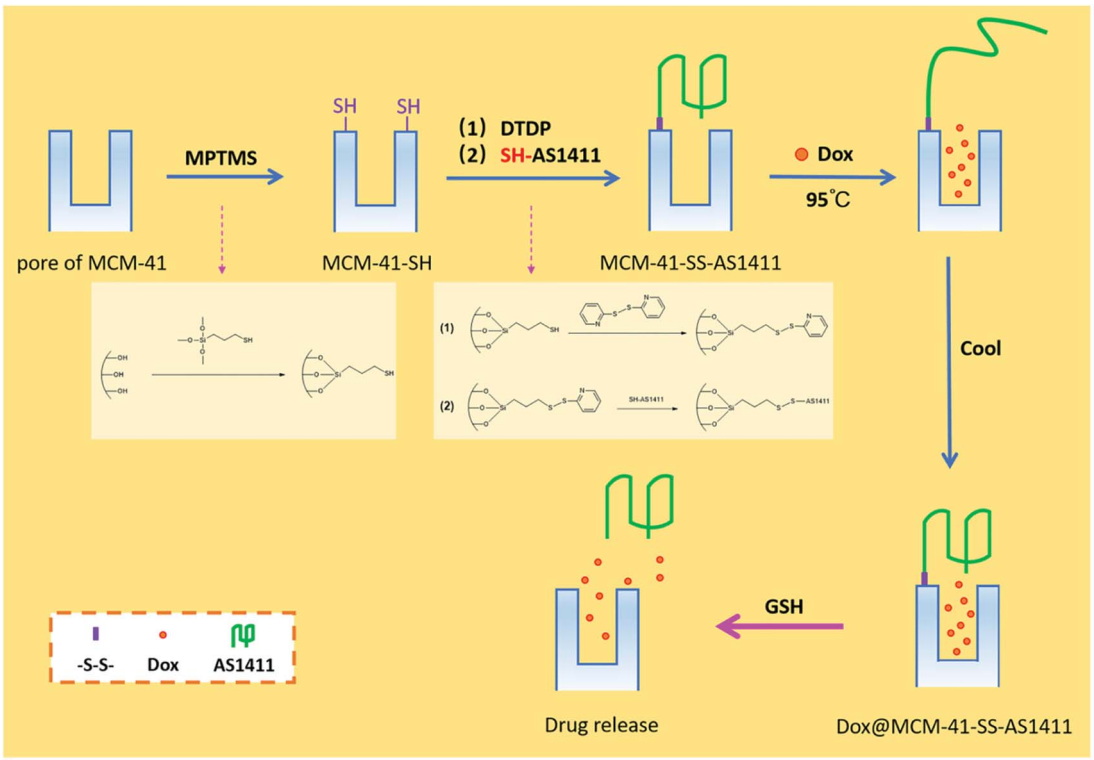

Scheme 1 Schematic illustration of the AS1411 aptamer nano-gatekeeper grafted and open at mesoporous silica pores.

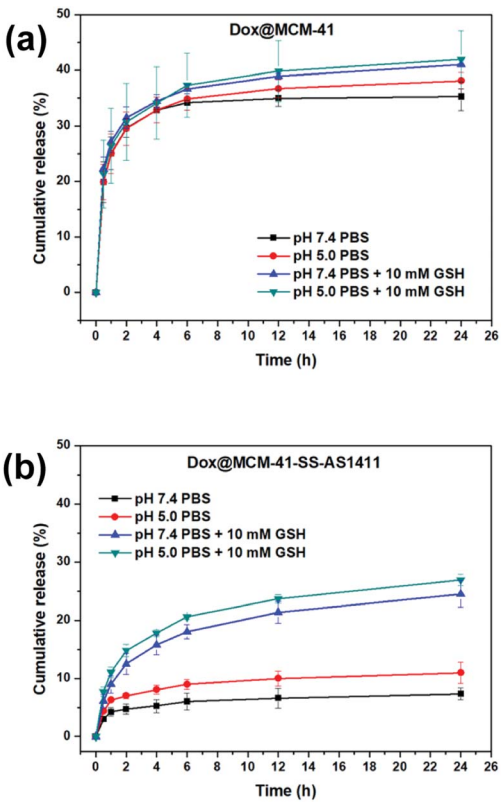

Fig. 5 The cumulative release rates of Dox with time in different pH environments with or without 10 mM GSH. (a) Non-gated DDS: Dox@MCM-41; (b) AS1411-gated DDS: Dox@MCM-41-SS-AS1411.

fluorescence detection. As illustrated in Table 3, the Dox amount loaded in AS1411-gated particles (MCM-41-SS-AS1411) was higher than that of bare MCM-41. AS1411 has a negative charge, and Dox has a positive charge in PBS solution.[28] Dox was attracted to AS1411 due to electrostatic interaction. Therefore, AS1411 also loaded some Dox in addition to MCM-41.

2.8 Investigation of GSH-controlled drug release

The GSH-controlled drug release process is as shown in Scheme 1. Aptamers gate the pores of MSNs through the disulfide bonds. When GSH is present, the disulfide bond can be broken by GSH, which makes the aptamer separate from the mesopores, so that Dox in the MSN carrier can gradually diffuse out.

As we all know, the microenvironment in tumors is generally more acidic than in normal tissues.[29] Normal blood remains constant at pH 7.4. While in tumor cells, pH is 5.5–6.0 in endosomes and 4.5–5.0 in lysosomes.[30,31] So in the research study, we use pH 7.4 PBS to simulate blood circulation and normal tissues, pH 5.0 PBS to simulate endosomes and lysosomes and 10 mM GSH solution to simulate GSH in intracellular fluid.

Fig. 5a shows the curve of Dox cumulative release from bare MCM-41 with time at pH = 7.4 or 5.0, with or without 10 mM GSH. As can be seen from the figure, Dox will release rapidly and massively when the MSN is not gated; there is little difference in the release of Dox in four different environments.

Fig. 5b shows the curve of Dox cumulative release from MCM-41-SS-AS1411 with time at pH = 7.4 or 5.0 with or without 10 mm GSH. As can be seen from the figure, there is a small amount of drug leakage in the absence of GSH. But the aptamer-

blocking effect is significant enough compared with the results in Fig. 5a. This may be because only one end of AS1411 is fixed on the surface of the carrier, and the other end is still open. The configuration of G-quadruplex may vary with different pHs, resulting in an inevitable small amount of leakage. But in general, it still played the role of a gatekeeper. In the presence of GSH, Dox release increased significantly. This shows that GSH can open the aptamer to release the drug, which reflects that the DDS can respond to GSH. As can be seen from Fig. 5b, in the acidic environment with pH = 5.0, the Dox released amount in the presence of GSH was slightly higher than that in the environment with pH = 7.4, which could be attributed to the increasingly acidic conditions which weakened the electrostatic interaction between Dox and the negatively charged carrier, resulting in more release in the pH = 5.0 environment.[28] This result suggested that the DDS could be beneficial for killing tumor cells and reducing damage to normal cells more or less.

As can be seen from Table 3 shown above, we found that MCM-SS-AS1411 had the higher drug loading capacity. However, comparing Fig. 5a and b, in the presence of GSH, MCM-SS-AS1411 displayed a lower amount of cumulative release rate than MCM-41 on the contrary. The reason was that AS1411 did not denature at 37 °C, which was the test temperature simulating the body temperature, and maintained its G-quadruplex configuration. So the Dox wrapped inside the spatial configuration of AS1411 was kept in it and difficult to release to the environmental media. Therefore, the cumulative drug release rates of MCM-SS-AS1411 were relatively lower than those of MCM-41 in the presence of GSH.

In summary, the MCM-41-SS-AS1411 drug delivery system can encapsulate the loaded drug molecules and release the drug in the presence of GSH.

3. Experimental

3.1 Synthetic procedures

3.1.1 Preparation of MCM-41-SH. MCM-41 particles were modified with thiol groups through silanization. The detailed preparation procedure is as follows. 0.25 g of MCM-41 and 2 mL trimethoxysilylpropanethiol (MPTMS) were dispersed in 15 mL dry toluene under a nitrogen atmosphere, and the mixture was shaken at room temperature for 24 h. The toluene was removed by heating in a rotary evaporator. Then the thiol-modified particle MCM-41-SH was obtained. The particles were washed thoroughly with ethanol and finally centrifuged and dried.

3.1.2 Preparation of aptamer-conjugated MSN (MCM-41-SS-AS1411). MCM-41-SH particles were grafted with aptamers which served as a nano-gatekeeper. Specifically, 20 mg MCM-41-SH and 800 μL DTDP (40 mg, 50 mg mL^{-1}, EtOH) were dispersed in 2 mL of anhydrous ethanol and stirred at room temperature overnight. The product was washed with ethanol thoroughly and dried. The pyridine-activated particles MCM-41-SS-Py were obtained. 5 mg MCM-41-SS-Py, 5.44 nmol of one end modified –SH aptamer AS1411 (denoted as SH-AS1411) and 2 mL H_2O were mixed together and stirred overnight at room temperature. Subsequently, the particles were collected by centrifugation and washed with water three times. The obtained particles were denoted as MCM-41-SS-AS1411.

3.1.3 Drug loading (Dox@MCM-41-SS-AS1411). For drug loading, a literature reported procedure was used.[32] In brief, 5 mg MCM-41-SS-AS1411 particles were mixed with 1.5 mL Dox (2 mg mL^{-1}) and stirred in a water bath at 95 °C for 2 h to introduce Dox into the pores. The mixture was further incubated at 70 °C for 0.5 h and 50 °C for 0.5 h, followed by incubation at room temperature for another 2 h to restore the spatial configuration of AS1411. Subsequently, the particles were thoroughly washed with pH 7.4 PBS several times to remove any drug molecules that were involuntarily adsorbed on the outside of the pores. The Dox-loaded particles were denoted as Dox@MCM-41-SS-AS1411.

3.1.4 Quantitative determination of the aptamer binding amount. The synthetic method is similar to that described in Section 3.1.2. But in this case, we used a fluorescence-labelled aptamer (denoted as SH-AS1411-Cy5). The so-called 'supernatant depletion method' was used to quantify the amount of aptamers immobilized on the pore outlets of MSN particles. The fluorescence intensity of the supernatant was measured with an excitation wavelength of 652 nm and an emission wavelength of 670 nm by using a fluorescence spectrophotometer. At the same time, 2.72 nmol of SH-AS1411-Cy5 were dissolved in 2.00 mL H_2O, and its fluorescence intensity was measured as a reference. Subsequently, the amount of unreacted aptamers in the supernatant was calculated by the comparison method. The number of aptamers conjugated to per particle was calculated by using eqn (1):[32]

$$N_{\mathrm{Apt}} = \frac{\left(n_{\mathrm{added}} - n_{\mathrm{supernatant}}\right) \times N_{\mathrm{A}}}{N_{\mathrm{particles}}} \quad (1)$$

where N_A is 6.02×10^{23}, $N_{particles}$ is the number of particles which was calculated by using eqn (2):

$$N_{\mathrm{particles}} = \frac{3m}{4d \times \pi R^3} \quad (2)$$

where m is the mass of particles, d is the particle's density of amorphous silicate (2.2 g cm^{-3}), and R is the radius.

3.1.5 Determination of Dox loading. All the supernatants were collected after each washing step, and the unloaded drugs in the supernatants were quantified by fluorescence detection. Then the drug loading capacity was calculated *via* formula (3):

$$\text{Loading capacity} = \frac{m_{\mathrm{added}} - m_{\mathrm{supernatant}}}{m_{\mathrm{particles}}} \quad (3)$$

3.2 Materials

MCM-41 particles were purchased from Nanjing XFNANO Materials Tech Co., Ltd (Nanjing, China). Trimethoxysilylpropanethiol (MPTMS, 99%) was received from Sigma-Aldrich. Toluene (99%) was purchased from Beijing Chemical Reagent Company. Glutathione (GSH, 98%), 2,2′-dithiodipyridine (DTDP, 98%) and Dox (98%) were obtained from Aladdin Chemical Inc. (Shanghai, China). Phosphate buffered saline (PBS, pH 7.4) was purchased from Huibai Biotech Co., Ltd (Shenyang, China). Aptamers were purchased from Sangon

Table 4 Aptamer sequences

Name	Sequences (5′ → 3′)
SH-AS1411	C_6SH-GGTGGTGGTGGTTGTGGTGGTGGTGG
SH-AS1411-Cy5	C_6SH-GGTGGTGGTGGTTGTGGTGGTGGTGG-Cy5

Biotech Co., Ltd (Shanghai, China), and the sequences are shown in Table 4.

All other chemicals were analytical grade and used without further purification. The buffer (PBS, pH 5.0) was prepared with ultrapure water produced from an ELGA PURELAB Classic water system (ELGA, UK).

3.3 Instrumentation

The TEM measurements were conducted using an FEI Tecnai G2 F30 transmission electron microscope (FEI, USA). Fourier transform infrared spectrophotometric (FTIR) spectra were recorded on a Cary 630 (Agilent, USA) spectrometer using the KBr pellet technique. Small-angle X-ray diffraction (SXRD) was performed on a SmartLab (RIGAKU, Japan). Thermogravimetric analysis (TGA) was performed on a TGA/DSC3+ instrument (METTLER TOLEDO, Switzerland) with a heating rate of 10 °C min^{-1} under a nitrogen flow. Zeta potentials were determined on a Nano-ZS90 laser particle size and zeta potential analyzer (Malvern, UK). The fluorescence spectra were examined with an F-7100 fluorescence spectrophotometer (Hitachi, Japan).

4. Conclusions

A redox-responsive controlled release drug delivery system was prepared by using MCM-41 type mesoporous silica as the drug carrier, AS1411 aptamers as the gatekeeper and each AS1411 fixed on the pore outlet of MCM-41 through one disulfide bond. We mainly aimed to demonstrate that the spatial volume of the G-quadruplex configuration of the AS1411 aptamer can be utilized to cap the pore of the DDS. The results of FTIR, SXRD and TGA show that AS1411 aptamers were successfully grafted on MCM-41. Quantitative analysis of the binding capacity of the aptamer showed that there were about 3.1×10^3 aptamers bonded to each carrier particle averagely. Taking Dox as the drug model, this DDS was studied to release drug by controlling the aptamer gatekeeper in the presence or absence of GSH under pH 7.4 and 5.0 conditions, respectively. The fluorescence detection results confirmed that MCM-41-SS-AS1411 can encapsulate drug molecules and can open the AS1411 gatekeeper to release Dox under the stimulation of 10 mM GSH. We hope this point of view of utilizing the volume of G-quadruplex configuration of AS1411 to cap the pore of the DDS can play a prompt role in relevant research.

Author contributions

Conceptualization, L. Z.; methodology, L. Z.; software, Y. Z.; investigation, L. Z.; validation, L. Z. and Y. Z.; writing, L. Z.; supervision, Y. M.; project administration, Y. M.; funding acquisition, Y. M. and L. Z. All authors have read and agreed to the published version of the manuscript.

Conflicts of interest

There are no conflicts to declare.

Acknowledgements

The authors thank the National Natural Science Foundation of China (Grant No. 21372262) and Basic Research Program of Higher Education of Liaoning Province of China (Grant No. LQNK201742). The Education Center for Medical Basic Experiment of China Medical University and China Medical University-The Queen's University of Belfast Joint College (CQC) are also gratefully acknowledged.

References

1 R. Guo, L. L. Li, W. H. Zhao, Y. X. Chen, X. Z. Wang, C. J. Fang, W. Feng, T. L. Zhang, X. Ma, M. Lu, S. Q. Peng and C. H. Yan, *Nanoscale*, 2012, **4**, 3577–3583.
2 C. H. Lee, S. H. Cheng, I. P. Huang, J. S. Souris, C. S. Yang, C. Y. Mou and L. W. Lo, *Angew. Chem., Int. Ed. Engl.*, 2010, **49**, 8214–8219.
3 J. Guo, Y. Wang, J. Wang, X. Zheng, D. Chang, S. Wang and T. Jiang, *Asian J. Pharm. Sci.*, 2016, **11**, 735–743.
4 W. Chen, P. Zhong, F. Meng, R. Cheng, C. Deng, J. Feijen and Z. Zhong, *J. Controlled Release*, 2013, **169**, 171–179.
5 C. Park, H. Kim, S. Kim and C. Kim, *J. Am. Chem. Soc.*, 2009, **131**, 16614–16615.
6 R. Cheng, F. Feng, F. Meng, C. Deng, J. Feijen and Z. Zhong, *J. Controlled Release*, 2011, **152**, 2–12.
7 G. Saito, J. A. Swanson and K.-D. Lee, *Adv. Drug Delivery Rev.*, 2003, **55**, 199–215.
8 Y. Zhao, J. L. Vivero-Escoto, I. I. Slowing, B. G. Trewyn and V. S. Lin, *Expert Opin.*, 2010, **7**, 1013–1029.
9 J. Wen, K. Yang, F. Liu, H. Li, Y. Xu and S. Sun, *Chem. Soc. Rev.*, 2017, **46**, 6024–6045.
10 J. S. Beck, J. C. Vartuli, W. J. Roth, M. E. Leonowicz, C. T. Kresge, K. D. Schmitt, C. T.-W. Chu, D. H. Olson, E. W. Sheppard, S. B. McCullen, J. B. Higgins and J. L. Schlenker, *J. Am. Chem. Soc.*, 1992, **114**, 10834–10843.
11 B. L. Haruo Takahashi, T. Sasaki, C. Miyazaki, T. Kajino and S. Inagaki, *Chem. Mater.*, 2000, **12**, 3301–3305.
12 E. Aznar, M. Oroval, L. Pascual, J. R. Murguia, R. Martinez-Manez and F. Sancenon, *Chem. Rev.*, 2016, **116**, 561–718.
13 M. R. Dunn, R. M. Jimenez and J. C. Chaput, *Nat. Rev. Chem.*, 2017, **1**, 0076.
14 A. D. Ellington and J. W. Szostak, *Nature*, 1990, **346**, 818–822.
15 N. Zhang, B. Liu, X. Cui, Y. Li, J. Tang, H. Wang, D. Zhang and Z. Li, *Talanta*, 2021, **223**, 121729.
16 R. R. White, B. A. Sullenger and C. P. Rusconi, *J. Clin. Invest.*, 2000, **106**, 929–934.

17 E. Levy-Nissenbaum, A. F. Radovic-Moreno, A. Z. Wang, R. Langer and O. C. Farokhzad, *Trends Biotechnol.*, 2008, **26**, 442–449.
18 K. W. Thiel and P. H. Giangrande, *Oligonucleotides*, 2009, **19**, 209–222.
19 L. T. Sa, S. Simmons, S. Missailidis, M. I. da Silva and R. Santos-Oliveira, *J. Drug Targeting*, 2013, **21**, 427–434.
20 M. Nejabat, M. Mohammadi, K. Abnous, S. M. Taghdisi, M. Ramezani and M. Alibolandi, *Carbohydr. Polym.*, 2018, **197**, 157–166.
21 Y. Li, Y. Duo, J. Bi, X. Zeng, L. Mei, S. Bao, L. He, A. Shan, Y. Zhang and X. Yu, *Int. J. Nanomed.*, 2018, **13**, 1241–1256.
22 Z. Peixian, Z. Shaoqiu, C. Ting and Z. Chunling, *J. Funct. Mater.*, 2017, **48**, 4049–4059.
23 P. J. Bates, D. A. Laber, D. M. Miller, S. D. Thomas and J. O. Trent, *Exp. Mol. Pathol.*, 2009, **86**, 151–164.
24 Y.-A. Shieh, S.-J. Yang, M.-F. Wei and M.-J. Shieh, *ACS Nano*, 2010, **4**, 1433–1442.
25 E. M. Reyes-Reyes, Y. Teng and P. J. Bates, *Cancer Res.*, 2010, **70**, 8617–8629.
26 A. Miranda, T. Santos, E. Largy and C. Cruz, *Pharmaceuticals*, 2021, **14**, 121.
27 Y. Zhang, J. Tan, L. Zhou, X. Shan, J. Liu and Y. Ma, *ACS Omega*, 2020, **5**, 31227–31233.
28 Y. Yang, Y. Lin, D. Di, X. Zhang, D. Wang, Q. Zhao and S. Wang, *J. Colloid Interface Sci.*, 2017, **508**, 323–331.
29 I. F. Tannock and D. Rotin, *Cancer Res.*, 1989, **49**, 4373–4384.
30 H. Wu, L. Zhu and V. P. Torchilin, *Biomaterials*, 2013, **34**, 1213–1222.
31 H. Yin, E. S. Lee, D. Kim, K. H. Lee, K. T. Oh and Y. H. Bae, *J. Controlled Release*, 2008, **126**, 130–138.
32 P. Sun, A. Leidner, S. Weigel, P. G. Weidler, S. Heissler, T. Scharnweber and C. M. Niemeyer, *Small*, 2019, **15**, 1900083.